NUMERICAL SIMULATION OF AIRFOIL ICE ACCRETION AND THERMAL ANTI-ICING SYSTEMS

Jeroen E. Dillingh, Harry W.M. Hoeijmakers
Group Engineering Fluid Dynamics, University of Twente
P.O. Box 217, 7500 AE, Enschede, The Netherlands
Phone/Fax: +31-53-4894428/3695, Email: j.e.dillingh@ctw.utwente.nl

Keywords: *Subsonic, Weather effects, Computational Fluid Dynamics*

Abstract

In this study, a computational method is presented that computes ice accretion on airfoils in specified icing conditions. A good agreement is found with the ice shapes predicted by other computational methods. Agreement with the experimental ice shapes is fair. Also, the implementation and application of a mathematical model of a thermal anti-icing system in the ice accretion simulation code 2DFOIL-ICE is presented. The numerical method has proven to be able to calculate the main parameters of an airfoil anti-icing system, such as: airfoil-skin temperatures (for the wetted region), runback water flow and convection heat transfer coefficient distributions along the external surface.

1 Introduction

Aircraft icing has long been recognized as a serious flight safety problem. Icing can occur when supercooled water droplets hit the aircraft, flying at a level where the temperature is at or below the freezing point. Ice accretion on the wing leading edge or on the tail plane can result in non-aerodynamic shapes and in serious degradation of the aerodynamic performance, such as a decrease in the stall angle, an increase in drag, a decrease in maximum lift, and altered moment characteristics of the aircraft. Also, ice accretion on parts of the engine nacelles or on propellers can cause dangerous situations.

Computer simulation of the ice accretion process provides an attractive method for determining the ice shapes on aircraft wings and evaluating a wide range of icing conditions. An ice accretion model that accurately predicts growth shapes on an arbitrary airfoil is valuable for analysis of the sensitivity of airfoils to ice accretion, and for analysis of the influence of variables such as airspeed and angle of attack to the accretion process. The predicted ice shapes can be used in wind tunnel and flight tests to assess aircraft performance and handling qualities degradation in icing conditions.

The same model can also be used to assess the energy requirements necessary to prevent ice build-up on an airfoil. Once a model has been validated, it will provide a cost effective means of performing most of the icing research studies which now rely upon experimental techniques.

Nowadays, it is common practice in the aircraft manufacturing industry to apply computational methods for ice accretion in two-dimensional flow for investigating icing. Studies to extend the two-dimensional ice growth model to three-dimensional flows are in progress at for example NASA GRC as well as at CIRA and ONERA. The 2DFOIL-ICE method [1,2] predicts the growth of ice on 2D surfaces. It is based on a quasi-steady model that takes into account all important mass and heat transfer processes that

occur when supercooled water droplets strike an airfoil. The droplets either freeze immediately upon impact or freeze partly while the rest of the water runs back on the airfoil. The capabilities of the method have recently been extended by the inclusion of a model for thermal ice protection systems. The use of this method, therefore, not only enables the assessment of potential icing hazards due to ice growth on unprotected surfaces but also the design and appropriate placement of thermal ice protection systems.

The objective of the present work is to compare numerical results and experimental data available from literature to the results obtained with 2DFOIL-ICE, for both ice accretion calculation and anti-icing simulation, in order to assess its value as an analysis tool for carrying out more studies to further elucidate the pertinent physical phenomena involved in the ice accretion and anti-icing process.

A brief review of the ice accretion model and the anti-icing system model is first presented. Then, the computational procedure is explained briefly. Finally, comparisons with other experimental and numerical results are made.

2 Ice Accretion

Due to the inertia the trajectories of the supercooled droplets will deviate from the streamlines, causing the droplets either to impinge on the airfoil or to be carried past it. The size, the shape and the location of the ice that will form depend on:

- the environmental parameters, such as ambient air temperature, pressure, cloud liquid water content (*LWC*), relative humidity and the median volumetric droplet diameter (*MVD*);
- the aircraft surface conditions, such as surface temperature, roughness and the surface tension at the air/water interface;
- the flow parameters, such as the flight velocity, angle of attack and the icing time.

Two distinct types of ice accretion have been observed:

- Rime-ice accretions: a dry, opaque and milky-white ice deposit with a density lower than that of the impinging droplets. It usually occurs at lower airspeeds, lower temperatures and lower *LWC*'s. In rime ice conditions the released latent heat of freezing is insufficient to raise the local temperature above the freezing point and all the droplets freeze fully upon impact. Generally, the rime-ice accretions have a streamlined form;
- Glaze-ice accretions: a heavy coating of a transparent ice which spreads over he wing and has a density close to that of the impinging droplets. It usually develops at higher airspeeds, temperatures closer to the freezing point and higher *LWC*'s. In glaze-ice conditions, due to the relatively high amount of released latent heat of freezing, only part of the water in the droplets freezes upon impact, the rest runs back along the airfoil surface. Generally, the ice formations have an irregular, non-aerodynamical shape which may jeopardize the aerodynamic characteristics of the airfoil section.

3 Droplet Trajectories

The following assumptions are made when considering the motion of an isolated droplet moving in a steady, non-uniform velocity field:

- the droplets are so small (10-50 μm) that they do not affect the velocity field induced by the airfoil in absence of the droplets;
- the droplet density and the droplet volume remain constant, implying that evaporation or other changes in phase do not take place;
- droplets are spheres, with a diameter equal to the equi-volumetric diameter d_{eq}, the diameter of a spherical droplet with the same volume;
- the initial droplet velocity equals the free stream velocity.

Droplets released upstream of the airfoil will tend to follow the streamlines up to some distance to the airfoil. Closer to the airfoil the flow will no longer be uniform. Due to the difference in density of the water and that of air, the changes in air velocity the droplet trajectories start to deviate from the streamlines. Since the relative velocity is low and the droplet size is small the flow around the droplet is a low-Reynolds-number flow. In considering the relative flow around a droplet, up to six different contributions to the force exerted on the droplet can be distinguished: the steady-drag force, the steady-lift force, the added-mass force, the pressure gradient force, the Basset motion history force and the buoyancy force.

Typically the steady-drag force is dominating the interaction forces and usually only this force and the buoyancy force (though very small) are used in Newton's second law that governs the droplet trajectory, i.e.

$$\frac{d\vec{x}_d}{dt} = \vec{u}_d$$

$$m_d \frac{d\vec{u}_d}{dt} = (\rho_d - \rho_a) V_d \vec{g} + \frac{1}{2}\rho_a A_d C_D \left|\vec{u} - \vec{u}_d\right| (\vec{u} - \vec{u}_d) \quad (1)$$

where m_d is the droplet mass, ρ_d is the droplet density, V_d is the droplet volume, ρ_a is the density of the air, $\vec{g}$ is the acceleration of the gravity, A_d is the droplet frontal area, C_D is the drag coefficient of the droplet, $\vec{u}$ denotes the local velocity of the air stream and $\vec{u}_d$ is the velocity of the droplet. Eq.(1) can be rearranged into:

$$\frac{d\vec{u}_d}{dt} + \frac{C_D Re_d}{24}\frac{18\mu_a}{d_{eq}^2 \rho_d}(\vec{u}_d - \vec{u}) = \left(1 - \frac{\rho_a}{\rho_d}\right)\vec{g} \quad (2)$$

where $Re_d = \rho_a \left|\vec{u} - \vec{u}_d\right| d_{eq}/\mu_a$ is the droplet Reynolds number. In very viscous (Stokes') flow the drag coefficient of a sphere is $C_D = 24/Re_d$. However, in the flows relevant to ice accretion the Reynolds numbers are not very low and a modified drag coefficient is used:

$$\frac{C_D Re_d}{24} = 1.0 + 0.197 Re_d^{0.63} + 2.6 \times 10^{-4} Re_d^{1.38} \quad (3)$$

This expression is accurate for Reynolds number up to 1000. The Reynolds numbers encountered in the applications do not exceed 100. Note that non-dimensionalizing Eq.(2), using $L_{ref} = c$, $U_{ref} = U_\infty$, $t_{ref} = c/U_\infty$, we find

$$\frac{d^2\vec{\xi}_d}{d\tau^2} + K\left(\frac{d\vec{\xi}_d}{d\tau} - \frac{\vec{u}}{\vec{U}_\infty}\right) = \left(1 - \frac{\rho_a}{\rho_d}\right)\frac{\vec{g}c}{U_\infty^2} \quad (4)$$

where $\vec{\xi}_d = \vec{x}_d/L_{ref}$, $\tau = t/t_{ref}$ and

$$K = 18\frac{C_D Re_d}{24}\frac{\rho_a}{\rho_d}\frac{1}{Re_c}\frac{1}{(d_{eq}/c)^2}$$

with $Re_c = \rho_a U_\infty c/\mu_a$ the airfoil Reynolds number. It shows that, apart from the density ratio ρ_a/ρ_d and the Froude number ($Fr^2 = U_\infty^2/cg$), the Langmuir parameter K is an important parameter. K represents the inertia effects: for large values of K the droplet velocity will tend to the air velocity $\vec{u}$ and the droplets will follow the streamlines. This implies that relatively small droplets ($d_{eq}/c \ll 1$), i.e. for large aircraft, icing will not be an important issue. However, for smaller aircraft, or for smaller parts of larger aircraft, icing will be important.

4 Flow Model and Thermodynamics

4.1 Control Volume

The amount of ice that accretes on the airfoil is computed by solving the heat and mass balances for small control volumes that are located along the airfoil surface. The physical model used in the present method is Messinger's method [3], applied in most present-day ice accretion prediction methods.

The equations that describe the thermodynamics of the freezing process are obtained by applying

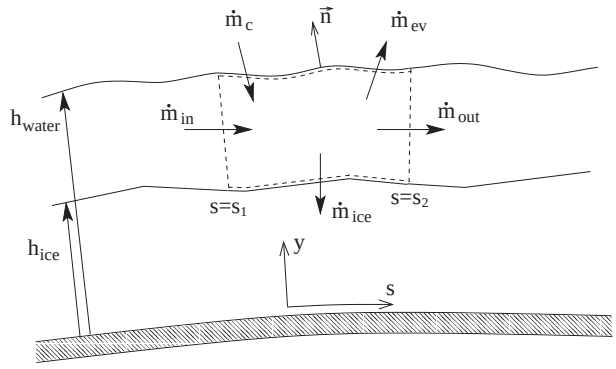

Fig. 1 The control volume with the mass flow rates

the continuity equation and energy conservation equation, for a steady flow and constant mass flow rates, to a small shallow control volume. The control volume is within the boundaries $s = s_1$, $y = h^-_{water}(s)$, $s = s_2$, $y = h^+_{ice}(s)$, where s is the coordinate along the surface, see Fig.1. The + and - sign indicate that the control volume boundary is just above and just below the interface, respectively. The two chord-wise boundaries coincide with the edges of the panels that constitute the airfoil. The lower boundary of the control volume is initially on the surface of the clean geometry, and moves outward with the surface as the ice accretes. Therefore, the control volume is always situated on either the clean or iced surface, and any accumulated ice is considered to leave the control volume through the lower boundary.

It should be noted that h_{ice} and h_{water} vary with time as a consequence of the ice accretion, but that they remain at the same relative distance due to the assumption of steady flow and constant mass flow rates.

For dimensional completeness, the control volume is considered to extend one unit length in the spanwise direction.

It is assumed that the control volume is so small that all physical variables can be taken constant in the control volume.

The only terms representing the motion of the water on the surface that are taken into account are $\dot{m}_{in}$ and $\dot{m}_{out}$, i.e. the rate of water flowing into the control volume out of the previous one and the rate of water flowing out of the control volume into the next one, respectively, both [kg/ms], that is [kg/s] per meter span. This means that there is a water transport along the surface, but that the water is assumed to have a velocity that can be neglected. This assumption is valid in cases where the velocities in the water layer are small. As a consequence of this assumption the equation describing conservation of momentum of the liquid water in the control volume is not used.

4.2 Conservation of Mass

The conservation of mass for water in an arbitrary control volume V with boundary ∂V moving with velocity $u_{\partial V}$ is (2D)

$$\frac{\partial}{\partial t}\int\int_V \rho_w \, dV + \int_{\partial V} \rho_w (\vec{u}_w - \vec{u}_{\partial V}) \cdot \vec{n} \, dS = 0 \tag{5}$$

where $\vec{n}$ is the unit normal vector on the surface of the control volume, pointing outwards.
Using the assumption of quasi-steadiness, the unsteady term drops out and, because of constant mass flow rates ($\vec{u}_{\partial V}$ = constant in space),

$$\int_{\partial V} \rho_w (\vec{u}_w \cdot \vec{n}) dS - \rho_w \vec{u}_{\partial V} \cdot \int_{\partial V} \vec{n} dS = 0 \tag{6}$$

which immediately reduces to

$$\int_{\partial V} \rho_w (\vec{u}_w \cdot \vec{n}) dS = 0 \tag{7}$$

The contributions to the contour integral term are $\dot{m}_{in}$, the mass flow of runback water into the control volume and $\dot{m}_{out}$, the mass flow of runback water out of the control volume, assuming that the variables are constant on each boundary of the control volume, i.e.,

$$\dot{m}_{in} = \int_{h^+_{ice}}^{h^-_{water}} \rho_w u_{in} dy \Big|_{s=s_1} \tag{8}$$

and

$$\dot{m}_{out} = \int_{h_{ice}^{+}}^{h_{water}^{-}} \rho_w u_{out} dy \Big|_{s=s_2} \tag{9}$$

To determine the contribution from the lower and upper boundary of the control volume, one has to perform a contour integral once again. The corresponding control volume is an infinitesimal control volume located on the interface, partially in the water and partially in the ice, or partially in the water and partially in the air. Such a control volume analysis couples the conditions on both sides of the interface. It is assumed that no splashing takes place and that the phase changes are instantaneous. The rate of ice that is formed is denoted by $\dot{m}_{ice}$, while the rate at which water evaporates at $y = h_{water}$ is denoted by $\dot{m}_{ev}$.

The mass flow rate into the control volume due to the droplets caught by the surface is expressed by

$$\dot{m}_c = LWC \cdot U_\infty \cdot \beta \cdot \Delta s \tag{10}$$

Here, LWC is the liquid water content of the air $\left[\mathrm{kg/m^3}\right]$. Δs is the length of the control volume along the surface [m]. β is the dimensionless local catching efficiency, defined as the ratio, for a given mass of water, of the area of impingement to the area through which the water passes at some distance upstream of the airfoil. The catching efficiency is found by computing the droplet trajectories and the droplet impact points.

The mass flow rate due to evaporation can be expressed in terms of the local temperature and pressure. In case there is no water on the surface there will be no evaporation. However, in that case, water can still leave the surface through sublimation of ice and $\dot{m}_{ev}$ is replaced by $\dot{m}_{sub}$, the rate of mass transfer through sublimation.

The mass balance then becomes

$$-\dot{m}_{in} + \dot{m}_{out} - \dot{m}_c + \dot{m}_{ev} + \dot{m}_{ice} = 0 \tag{11}$$

All terms are in units of [kg/ms], that is [kg/s] per meter span.

The concept of a freezing fraction can be used to determine the type of process taking place within the control volume. The freezing fraction, f, was defined by Messinger [3] as the fraction of impinging liquid that freezes within the region of impingement,i.e.,

$$f = \frac{\dot{m}_{ice}}{\dot{m}_c} \tag{12}$$

The remaining water runs along the surface. In the present study, f is defined as the fraction of the total mass of water entering the control volume that freezes within the control volume. It is given by

$$f = \frac{\dot{m}_{ice}}{\dot{m}_c + \dot{m}_{in}} \tag{13}$$

For colder (rime) icing conditions, the droplets tend to freeze immediately on impact, resulting in zero runback. In that case, neglecting sublimation, the freezing fraction equals 1.0. Freezing fractions equal to 0.0 indicate that no ice has formed in the control volume. Freezing fractions between 0.0 and 1.0 characterize glaze ice or ice that has some combination of glaze and rime characteristics. The local value of f can vary along the surface, and can be calculated from the control-volume mass and energy balance. Fig.2 shows the three phase-regimes that can be distinguished. The freezing fraction acts as a phase-regime indicator.

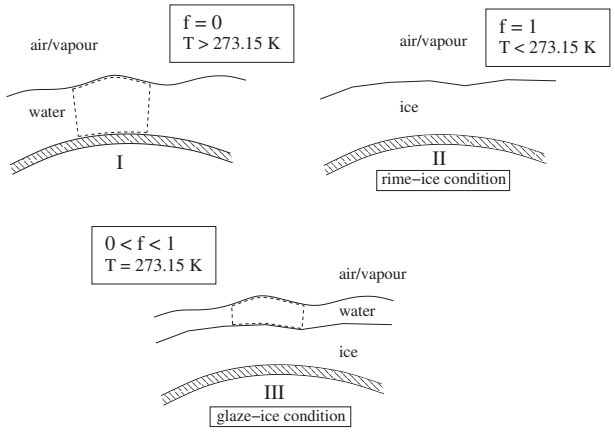

Fig. 2 The three phase-regimes

4.3 Conservation of Energy

The conservation of energy within the control volume can be treated in the same way as the conservation of mass. In the energy equation the work done by frictional forces within the water and the work done by external force fields are neglected, while it is assumed that there are no volumetric heat sources. This leads to:

$$\int_{\partial V} \rho_w H_w (\vec{u}_w \cdot \vec{n})\, dS = -\int_{\partial V} \vec{q}_w \cdot \vec{n}\, dS \qquad (14)$$

with H_w the total enthalpy and $\vec{q}_w$ the heat flux. When considering the enthalpy of the runback water that flows into the control volume, out of the preceding control volume, the kinetic energy is not taken into account, i.e.

$$\dot{m}_{in} H_{w,in} = \int_{h_{ice}^{+}}^{h_{water}^{-}} \rho_w h_{w,in} u_{in} dy \Big|_{s=s_1} \qquad (15)$$

Similarly, in the enthalpy of the water leaving the control volume, the kinetic energy is not taken into account,

$$\dot{m}_{out} H_{w,out} = \int_{h_{ice}^{+}}^{h_{water}^{-}} \rho_w h_{w,out} u_{out} dy \Big|_{s=s_2} \qquad (16)$$

An expression for the contributions associated with droplet catching, evaporation and freezing is obtained from the second control volume analysis. The heat flux due to convection at the air/water interface:

$$q_{conv} \Delta s = \int_{s_1}^{s_2} \vec{q}_{conv,w} \cdot \vec{n} ds \Big|_{h=h_{water}^{-}} \qquad (17)$$

Note that the convective heat flux is commonly referred to as 'convective', although it follows from a heat conduction term.

It is assumed that the radiative heat flux can be neglected, while also the heat flux through the boundary at $s = s_1$ and the one at $s = s_2$ due to conduction can be neglected. There is no heat flux through the lower boundary of the control volume, since as soon as ice has accreted any heat transfer between the water and the ice and between the ice and the airfoil skin will be very small since ice is an insulator. In case both ice and water are present on the airfoil, the temperature of the ice and the water will be 273.15 K and there will be no convective heat flux between the water and the ice. The right-hand side of Eq.(14) is then,

$$-\int_{\partial V} \vec{q}_w \cdot \vec{n}\, dS = -q_{conv} \Delta s \qquad (18)$$

with

$$q_{conv} = h_c \left(T_{sur} - \left(T_e + r \frac{U_e^2}{2 c_{pa}} \right) \right) \qquad (19)$$

the convective heat flux per unit area $[\mathrm{W/m^2}]$, with h_c the convective heat transfer coefficient and r the recovery factor. T_e and U_e are the temperature and velocity outside the control volume at the edge of the air boundary layer, respectively. The local temperature T_e is calculated from the pressure calculated by the potential flow method using the isentropic relations. T_{sur} is the temperature of the water in the control volume. Δs is the length of the control volume along the surface. (The conduction through the skin of the airfoil is introduced later when considering the thermal anti-icing model.) Substituting and writing out the different terms, assuming the specific heat of water and that of ice to be constant, and using Eq.(11), we find

$$\begin{aligned} \dot{m}_{ev} h_{WV/IV}^{T_{ref}=T} + q_{conv} \Delta s = & \\ & \dot{m}_c [c_{pw} (T_\infty - T) + U_\infty^2/2] \\ + \; & \dot{m}_{in} [c_{pw} (T_{in} - T)] \\ + \; & \dot{m}_{ice} h_{IW}^{T_{ref}=T_f} - \dot{m}_{ice} c_{pw} (T_f - T) \\ + \; & \dot{m}_{ice} c_{pi} (T_f - T) \end{aligned} \qquad (20)$$

with $T_f = 273.15$ K. T_{ref} is the reference temperature and $T = T_{sur} = T_{out}$. The subscript (w) denotes the water phase, the subscript (v) denotes the vapour phase, the subscript (i) denotes the ice phase, and the subscript (a) denotes the property of air. $h_{WV}^{T_{ref}=T}$ is the latent heat of vaporisation of water at temperature T, $h_{IV}^{T_{ref}=T}$ is the latent heat of sublimation. All terms are in units of $[\mathrm{W/m}]$,

that is [W] per meter span.

With reference to Vukits [4], Eq.(20) is expressed in the form

$$\dot{Q}_{Source} = \dot{Q}_{Sink} \tag{21}$$

where $\dot{Q}_{Source}$ represents the heat flux from sources and $\dot{Q}_{Sink}$ represents the heat flux from sinks. A source provides heat to the control volume. A sink represents a process that removes heat from the control volume.

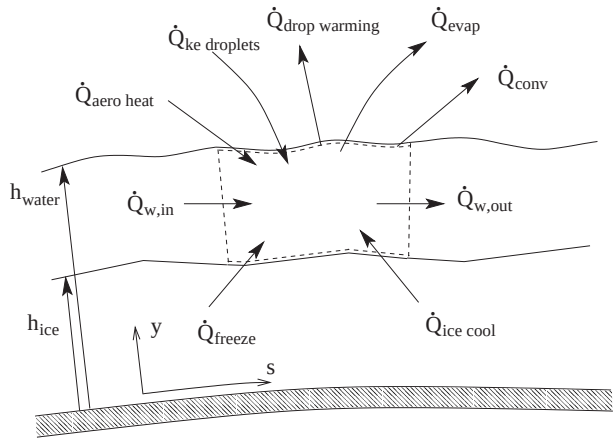

Fig. 3 The control volume with the heat fluxes

Assuming that the surface skin temperature is higher than the temperature of the air and the droplets ($\dot{Q}_{drop\,warming}$ is a sink), the sources of heat are (see Fig.3),

$$\begin{aligned}\dot{Q}_{Source} &= \dot{Q}_{in} + \dot{Q}_{freeze} + \dot{Q}_{aero\,heat} \\ &\quad + \dot{Q}_{ke\,droplets} + \dot{Q}_{ice\,cool}\,(+\dot{Q}_{anti-ice})\end{aligned} \tag{22}$$

where

$$\begin{aligned}\dot{Q}_{in} &= \dot{m}_{in} c_{pw} (T_{in} - T) \\ \dot{Q}_{freeze} &= \dot{m}_{ice} h_{IW}^{T_{ref}=T_f} + \dot{m}_{ice} c_{pw} (T - T_f) \\ \dot{Q}_{ke\,droplets} &= \dot{m}_c \frac{U_\infty^2}{2} \\ \dot{Q}_{ice\,cool} &= -\dot{m}_{ice} c_{pi} (T - T_f) \\ \dot{Q}_{aero\,heat} &= h_c \left(T_e + r \frac{U_e^2}{2 c_{pa}} - T_\infty \right) \Delta s\end{aligned}$$

Again, $T = T_{sur} = T_{out}$. The heat flux due to conduction, $\dot{Q}_{anti-ice}$, comes into play in the anti-icing model.

The heat sinks are as follows (see Fig.3),

$$\dot{Q}_{Sink} = \dot{Q}_{conv} + \dot{Q}_{drop\,warming} + \dot{Q}_{evap} + \dot{Q}_{out} \tag{23}$$

where

$$\begin{aligned}\dot{Q}_{conv} &= h_c (T_{sur} - T_\infty) \Delta s \\ \dot{Q}_{drop\,warming} &= -\dot{m}_c c_{pw} (T_\infty - T_{sur}) \\ \dot{Q}_{evap} &= \dot{m}_{ev} h_{WV}^{T_{ref}=T_{sur}} \\ \dot{Q}_{out} &= c_{pw} \dot{m}_{out} (T_{out} - T_{sur})\end{aligned}$$

All terms substituted in Eq.(21) yields:

$$\begin{aligned}&\dot{Q}_{in} + \dot{Q}_{freeze} + \dot{Q}_{ke\,droplets} + \dot{Q}_{ice\,cool} \\ &\quad + \dot{Q}_{aero\,heat}\,(+\dot{Q}_{anti-ice}) = \\ &\quad \dot{Q}_{conv} + \dot{Q}_{drop\,warming} + \dot{Q}_{evap} + \dot{Q}_{out}\end{aligned} \tag{24}$$

5 Numerical Approach

As soon as ice starts to accrete on the airfoil, the flow around the airfoil will change because of the change in shape of the iced airfoil. In turn a different flow field will lead to a change in the ice accretion process, since there will be an influence on the droplet trajectories, the catching efficiency, the convective heat transfer coefficient, etc. This implies that the ice accretion process is a time-dependent process and requires the solution of time-dependent equations. However, the changes in time are slow and we adopt a quasi-steady approach in which the ice accretion is computed layer by layer, assuming a steady flow field during the growth of each layer. The algorithm consists of four steps:

- computation of the flow field;
- computation of the limiting droplet trajectories and the impingement parameters;
- solution of the mass and the heat balances along the airfoil surface;
- definition of a new, iced airfoil shape.

5.1 Computation of the Flow Field

Starting with the appropriate airfoil and environmental data, the flow field around the airfoil is

calculated. At high Reynolds number, low Mach number and for not too ragged ice shapes the flow around the airfoil section may be described by the incompressible potential flow model, governed by Laplace's equation for the velocity potential. The computational method 2DFOIL [2,5] is used to compute the flow field around the airfoil. 2DFOIL is a second-order accurate panel method for the two-dimensional unsteady, incompressible potential flow around arbitrary airfoil shapes. An airfoil cross section is divided into a large number of (curved) segments of varying lengths, employing a curvature-dependent paneling scheme. Considerably more airfoil segments are defined near the leading edge where ice accretion is anticipated.

2DFOIL employs a panel-wise linear source distribution, a panel-wise quadratic doublet distribution and accounts for the curvature of the surface. The singularity distributions are solved for by imposing the Dirichlet condition that in the interior of the airfoil section the perturbation potential equals zero, at the midpoint of each panel. The velocities around the airfoil and on the airfoil surface follow from the calculated source and doublet distribution.

Panel methods are known to be very reliable numerical tools to compute the flow field and the pressure distribution in regions away from the airfoil or at specific points on the airfoil itself such as the collocation points. Care should be taken when the panel method is used to compute the droplet trajectories close to the paneled surface of the airfoil, for only at the collocation points the zero-normal-velocity boundary condition is met exactly. Away from the collocation points a nonzero normal velocity may arise. Furthermore, close to the panel edges the discontinuities in the geometry and in the singularity distributions result in a (logarithmic) singular velocity field, i.e. in a locally very high, unrealistic, value of the velocity.

In the present higher-order panel method this problem is considerably less severe than for lower-order panel methods. The problem is further reduced by pursuing the following approach. If a droplet is within a certain distance (determined to be three panel widths) away from the airfoil, the nearest panel and its two neighbors are each divided in N sub-panels. The parameters required in the definition of the linear source and quadratic doublet distribution on the sub-panels are obtained from the computed source and doublet distribution on the original panels by linear and quadratic interpolation, respectively. Subsequently the velocity induced by the (known) singularity distributions on the sub-paneled geometry is computed, which yields a smooth behavior of the velocity along the trajectory.

5.2 Convective Heat Transfer

In order to compute the convective heat transfer coefficient h_c, the boundary layer properties are required. In the present method linear interpolation in the tangential velocity component is used to find the stagnation point. During ice accretion irregular shapes may evolve for which a potential flow method produces questionable results, such as the appearance of multiple stagnation points and regions with high velocities. In order to cope with the multiple stagnation points the present method uses the following approach: on each new layer of ice all points where the tangential velocity is zero are determined. The stagnation point on the new layer is chosen as the point closest to the stagnation point on the old ice shape.

Employing the Reynolds analogy, the heat convection coefficient is obtained from the Blasius expression for the turbulent flat-plate boundary layer,

$$h_{c,BL}(s) = 0.0296\,\hat{f}\,\frac{\kappa}{s} Pr^{\frac{1}{3}} Re_s^{\frac{4}{5}} \qquad (25)$$

with Pr the Prandtl number $Pr = \mu_a c_{pa}/\kappa$; Re_s the Reynolds number based on the distance s from the stagnation point and using the local velocity from the potential method $Re_s = sU_e(s)/\nu_a$; and the factor $\hat{f}$ has been chosen equal

to 2, which gave the best agreement between calculated ice shapes and ice shapes found in experiments. In the stagnation region the lower bound of the heat convection coefficient is taken to be

$$h_c^{stag} = \frac{1}{2}\kappa\left(\frac{1}{\nu_a}\frac{dU_e}{ds}\right)^{\frac{1}{2}} \tag{26}$$

with dU_e/ds the velocity gradient at the boundary layer edge.

5.3 Droplet Trajectories

Droplet trajectories are calculated in the potential flow field using the appropriate mean cloud droplet diameter. From the location of the impacts of the various trajectories on the airfoil, local values of water droplet catching efficiency are calculated around the airfoil.

The droplet trajectories are obtained from Eq.(2), using Eq.(3), employing a five-stage Runge-Kutta scheme to integrate the equations in time. The time step in the method is adapted such that the CFL condition is satisfied, the time step is smaller than a specified maximum and the position of the droplet does not change more than a specified maximum. The time step also depends on the curvature of the trajectory.

A droplet is considered to have impacted when its trajectory intersects one of the panels. To determine the impact point the droplet velocity at the point on the trajectory just prior to intersection is used to extrapolate the droplet trajectory to the surface.

First, the two limiting droplet trajectories are determined, one that just hits the upper surface and one that just does not miss the lower surface. All droplets are released at 1.5 chords upstream of the leading edge of the airfoil.

Next, a number of droplets are released in between the lower and upper limiting trajectories and the impact points on the airfoil are determined. In this way a relation is found between the vertical coordinate of the release point $y_0(s)$ and the curvilinear distance s from the stagnation point to the impact point.

Taking a unit width as one dimension of both area terms (i.e., 1 m in spanwise direction), the local catching efficiency can then be defined as,

$$\beta = \frac{dy_0}{ds} = \frac{\Delta y_0}{\Delta s} \tag{27}$$

where Δy_0 is the spacing between the starting positions of two water droplets at the release location and Δs is the distance along the body surface between the impact locations of the same two droplets, see also Fig.4. The local values of $\beta(s)$ are obtained by finding, at each impact point, the derivative of $y_0(s)$ from the spline fitted through the impact point and its immediate neighbors. At the two end points, which determine the impingement region, β becomes zero. Finally, the value of β at the panel midpoints is obtained by linear interpolation between the values of β found at the two nearest impact points.

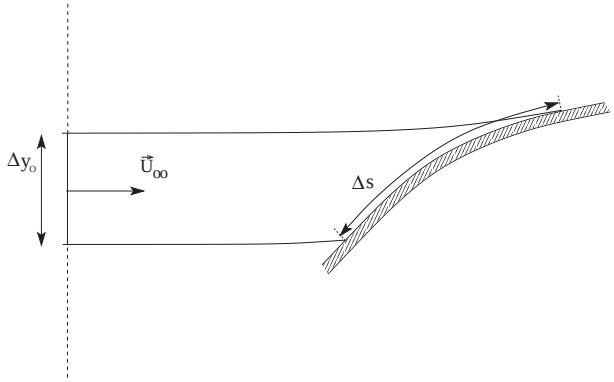

Fig. 4 Schematic for calculating β

5.4 Heat and Mass Balance

The local catching efficiency is necessary input for the mass and energy balance ice growth model. It, along with the free stream velocity U_∞ and the cloud liquid water content LWC, determines how much water impinges on the local region of the surface considered. Variations in the local catching efficiency can significantly alter the ice growth for that surface region. Using

local catching efficiencies and the environmental conditions of free stream temperature, cloud liquid water content, and relative humidity, thermodynamic calculations are made which determine the rate of ice growth at each segment around the airfoil defining the surface. It is noted that the (shallow) control volumes of the mass and heat balances are lined up with the panels used in the panel method, except for the panel on which the stagnation point is located. The latter panel has two control volumes, one at either side of the stagnation point.

The mass balance, see Eq.(11), is

$$-\dot{m}_{in} + \dot{m}_{out} - \dot{m}_c + \dot{m}_{ev}(T) + \dot{m}_{ice} = 0 \quad (11b)$$

and the heat balance, governing all three phase-regimes, see Fig.2, (see Eq.(20))

$$\begin{aligned} \dot{m}_{ev}(T) h_{WV/IV}^{T_{ref}=T} + q_{conv}(T)\Delta s = & \\ & \dot{m}_c[c_{pw}(T_\infty - T) + U_\infty^2/2] \\ + \quad & \dot{m}_{in}[c_{pw}(T_{in} - T)] \\ + \quad & \dot{m}_{ice} h_{IW}^{T_{ref}=T_f} - \dot{m}_{ice} c_{pw}(T_f - T) \\ + \quad & \dot{m}_{ice} c_{pi}(T_f - T) \end{aligned} \quad (20b)$$

For known $\dot{m}_{in}$, there are three unknowns: $\dot{m}_{out}$, $\dot{m}_{ice}$, $T = T_{sur}$, but only two equations. All terms in the energy balance are a function of the surface temperature. The evaluation of Eqs.(11b) and (20b) starts at the control volume next to the stagnation point where $\dot{m}_{in}$ equals zero. All terms in Eq.(20b) are then evaluated for $T = T_f$ and the equation is solved for $\dot{m}_{ice}$, the rate at which ice accretes. The freezing fraction f then follows from its definition.

If $0 \leq f \leq 1$ (phase-regime III in Fig.2), the initial guess of $T = T_f$ was correct and $\dot{m}_{out}$, the mass flow rate leaving the control volume follows from Eq.(11b).

If $f > 1$ (phase-regime II), i.e. all incoming water freezes and $\dot{m}_{ice} = \dot{m}_{in} + \dot{m}_c$. In this case, T follows from Eq.(20b).

If $f < 0$ (phase-regime I), no water freezes, i.e. $\dot{m}_{ice} = 0$ and the temperature T follows from Eq.(20b).

When the thermodynamic characteristics of the control volume are known and $\dot{m}_{ice}$ is determined, the mass balance is used to determine the mass flow rate of runback water $\dot{m}_{out}$, out of the control volume. Any water flow out of the control volume will be away from the stagnation point and into the next control volume.

The above procedure is then repeated for the adjacent downstream control volume, for which we now know $\dot{m}_{in}$, and continued along the upper surface of the airfoil. The entire procedure is then repeated again, starting at the stagnation point and proceeding along the lower surface of the airfoil.

5.5 Definition of the New Ice Shape

The ice growth rate $\dot{m}_{ice}$ is assumed to apply to a certain time interval Δt. The local ice thickness follows from

$$\Delta h_{ice} = \frac{\dot{m}_{ice}\Delta t}{\rho_{ice}\Delta s} \quad (28)$$

The density ρ_{ice} of ice follows from an empirical relation involving the *MVD*, the droplet velocity at impact, the surface temperature T and the freezing temperature T_f, see [2]. The magnitude of Δt depends amongst others on the cloud liquid water content and air velocity. The time scale of the ice accretion process is much larger than the time scale of the airflow. This allows the flow conditions to be considered steady and the flow rate of the ice growth to be considered constant during an icing step.

The calculated ice thickness is added to the body in the direction normal to the surface. When the added layer thicknesses are found for all segments, the airfoil shape is updated. Subsequently, these discrete points are used in a curvature-dependent adaptive paneling scheme to accurately re-discretize the iced airfoil contour for

the computation of the new velocity field. Then, a new time step is started. The flow field and catching efficiency computations are repeated after each update of the airfoil shape until the desired icing time has been reached.

6 Anti-Icing

Usually, anti-icing systems keep the cold water impinging on the aircraft above the freezing point. The heat for this comes from electrical pads installed in the metal skin or from hot air impinging on the metal skin inside the front part of the body to be protected. In the case of wings, anti-icing systems are installed in the leading edge area where water impinges. Although it is possible to keep the leading edge area just above freezing point so that the water freezes further downstream, most of the anti-icing systems are designed to evaporate a large part of the impinging water.

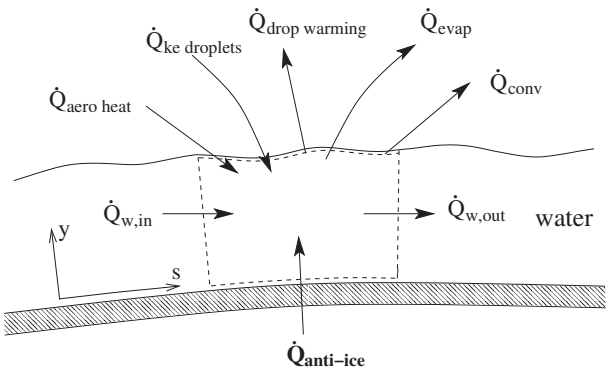

Fig. 5 The heat fluxes in the anti-icing model

To allow for heat conduction through the skin of the airfoil, an extra term is added to the heat balance,

$$\begin{aligned}\dot{m}_{ev}h_{WV}^{T_{ref}=T} + q_{conv}\Delta s - q_{anti-ice}\Delta s = \\ \dot{m}_c[c_{pw}(T_\infty - T) + U_\infty^2/2] \\ + \dot{m}_{in}[c_{pw}(T_{in} - T)] \\ + \dot{m}_{ice}h_{IW}^{T_{ref}=T_f} - \dot{m}_{ice}c_{pw}(T_f - T) \\ + \dot{m}_{ice}c_{pi}(T_f - T)\end{aligned} \tag{29}$$

where $q_{anti-ice}\Delta s$ is the heat transfer at the bottom of the control volume, see Fig.5.

Since the melting of previously deposited ice from the surface of the body is not modeled, the equations are not applicable to a de-icing system. They are applicable, however, to the evaluation of a thermal anti-icing system. A thermal anti-icing system differs from a de-icing system in that sufficient heat is supplied to prevent any ice from forming.

Now that a new variable is introduced in the heat balance, it brings, for known $\dot{m}_{in}$, the total number of unknowns to 4, i.e. $\dot{m}_{out}$, $\dot{m}_{ice}$, T and $q_{anti-ice}$. However, one of these 4 quantities is preset to a certain value.

The first way to use the anti-icing method is to specify the surface temperature T, say at a value larger than T_f, which is the same for every location along the surface of the protected area. In this case, $\dot{m}_{ice}$ is set to zero and the phase-regime is considered in which there is only water present on the surface. In this way, the number of unknowns reduces to 2, i.e. $\dot{m}_{out}$ and $q_{anti-ice}$. With the mass balance and the heat balance the system can be solved. The heat flux $q_{anti-ice}$, required to keep the surface temperature at its preset level, is a result from the calculation. The analysis stops when, marching from the stagnation point to the trailing edge, the point is reached where there is no impinging water and also no runback water left, i.e. the runback water limit. Beyond this point the airfoil is dry. (The plotted results will therefore not extend beyond these points.)

It is also possible to specify the edges of the protected surface. The control volume containing an edge point is split into two parts. The derived quantities in the new panel midpoints are calculated from interpolated values of velocity obtained from the panel method. The control volume analysis on the protected part applies to the all-water phase-regime, while the analysis for the other part allows all three phase-regimes, see Fig.6. The positions of the runback water limits

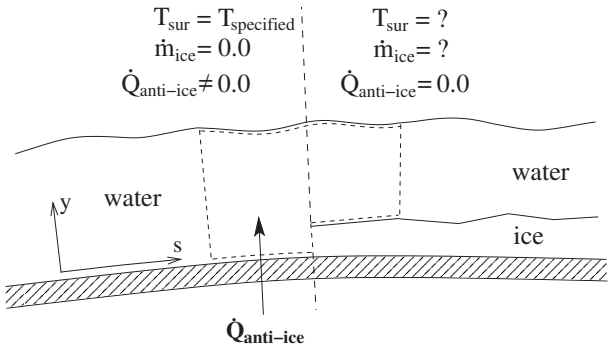

Fig. 6 Control volume analysis near the edge of the protected surface

relative to the limits of the protected surface help the user of 2DFOIL-ICE to distinguish between a 'running-wet' system and a 'fully-evaporative' system.

The second way to use the method is to specify a heat flux $q_{anti-ice}$ to simulate the heat addition by means of an electro-thermal anti-icing system. 2DFOIL-ICE is to be applied to determine whether this heat flux is sufficient to maintain an ice-free surface at the specified set of icing conditions. If it is possible for ice to form aft of the heater, this result indicates that the heat flux should be increased in this region to maintain an ice-free surface. The same procedure for calculating the ice shape is repeated here. $\dot{m}_{ice}$ is not set to zero, but is now a result from the calculation. If it appears that $\dot{m}_{ice}$ within the protected area is not equal to zero, then one has to conclude that the anti-icing system has failed, since the heat supplied has not been sufficient to avoid ice formation. The surface temperature is also a result of the calculations.

7 Convective Heat Transfer Coefficient

In the anti-icing model, and for the test case considered in this study, the expression for the convective heat transfer coefficient is somewhat different from the expression used in the ice accretion prediction model. Now, expression Eq.(25) applies to the region of the airfoil not close to the leading edge.

Around the stagnation point, a different expression for h_c is used. The nose of the airfoil is approximated by a 2D cylinder with diameter D, two times the leading-edge radius of curvature. Frössling [6] developed the following series expansion for h_c (iso-thermal wall)

$$h_{c,FR}(s) = h_c^{stag}(s)\left(1+4\frac{u_3}{u_1}\frac{F_2'}{F_0'}\left(\frac{s}{D}\right)^2 +6\frac{u_5}{u_1}\left(\frac{G_4'}{F_0'}+\frac{u_3^2}{u_1u_5}\frac{H_4'}{F_0'}\right)\left(\frac{s}{D}\right)^4+\cdots\right) \tag{30}$$

with

$$F_0' = -0.4959 \qquad u_1 = 2\left(2-\frac{5}{6}M_\infty^2\right)$$
$$F_2' = -0.1119 \qquad u_2 = 8\left(-\frac{1}{3}+\frac{77}{36}M_\infty^2\right)$$
$$G_4' = -0.0977 \qquad u_3 = 32\left(\frac{1}{60}+\frac{145}{144}M_\infty^2\right)$$
$$H_4' = \quad 0.0318$$

and $\frac{s}{D} = \frac{1}{2}\phi$, with ϕ the angle measured from the stagnation point and M_∞ the free stream Mach number.

While the Blasius expression only applies to the aft region of the airfoil, the validity of Eq.(30) is confined to a region near the stagnation point. A blending between Eq.(30) and Eq.(25) is introduced for the region in between,

$$h_c(s) = \begin{cases} h_{c,FR}(s) & 0 < s < s_C \\ (1-\alpha(s))\,h_{c,FR}(s_C) + \alpha(s)h_{c,BL}(s_{FP}) & s_C < s < s_{FP} \\ h_{c,BL}(s) & s_{FP} < s < 1 \end{cases}$$

with $\alpha(s) = (s-s_C)/(s_{FP}-s_C)$. s is the normalized curvilinear distance along the airfoil surface from the stagnation point. s_C is defined by ϕ_C, which is set to $\pi/4$ for a NACA 0012 airfoil, see Fig.7. Between $s = 0$ and $s = s_C$, the nose of the airfoil is approximated by a cylinder. The distance between s_{FP} and s_C can be modified by the user of 2DFOIL-ICE. It represents a transition region with a defined length in which the flow turns from the laminar into the fully turbulent regime.

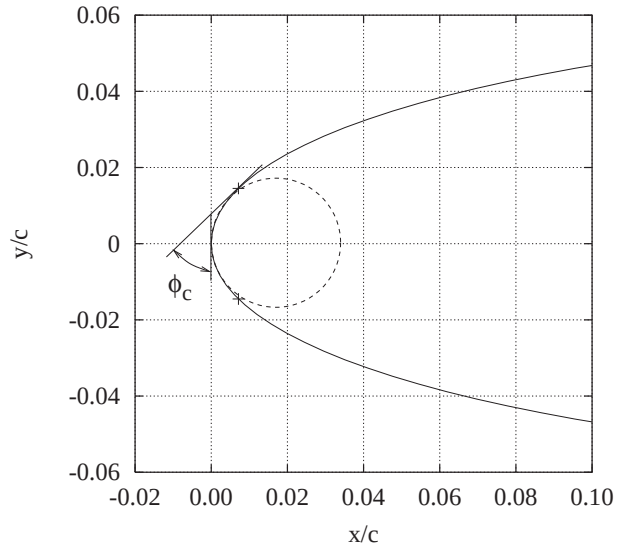

Fig. 7 Nose of NACA 0012 airfoil approximated by cylinder

Case Title	U_∞ [m/s]	T_∞ [^{o}C]	LWC [g/m^3]	MVD [μm]	Time [s]
C-7	69.87	257.43	1.16	20	517.10
C-9	92.54	257.60	0.33	20	1224.0

Table 1 Parameters of the two cases studied

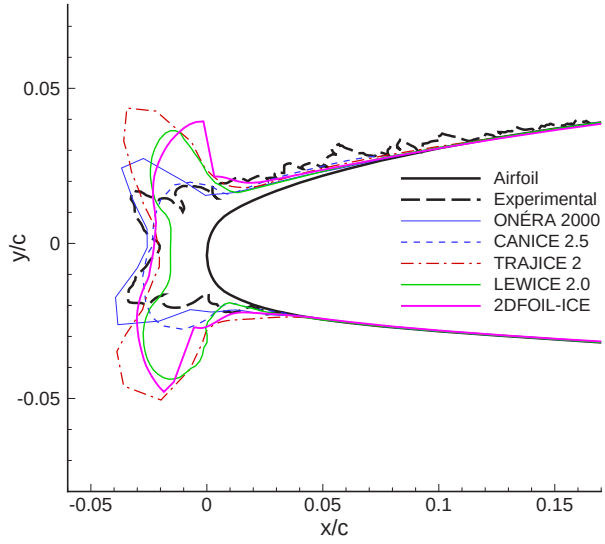

Fig. 8 The calculated ice shape for case C-7

8 Results

To validate the ice accretion prediction capability of the 2DFOIL-ICE code, two test cases are considered for which experimental data are available. The test case parameters are presented in Table 1, test case C-7 for a GLC305 airfoil and test case C-9 for a NLF0414 airfoil, both with a chord of 0.9144 m and zero angle of attack. The experimental results were obtained at the NASA Glenn Icing Tunnel. Both cases are taken from the NATO/RTO TR-038 Workshop (AVT Task Group 2001). Fig.8 shows the calculated ice shape for case C-7 and Fig.9 for case C-9. Solutions from some of the workshop participants are also included for comparison. It is noted that in our computation of the ice shape no tuning has been applied to get a closer match with the experimental ice shape, i.e. the comparison is 'blind'.

These results demonstrate that for these cases 2DFOIL-ICE gives results comparable to the results of other prediction methods, agreement with the experimental results is only fair.

The anti-icing method has also been validated using the experimental surface temperature distribution obtained by Al-Khalil *et al.* [7] The experimental results were obtained on a NACA 0012 airfoil, 6 ft (1.829 m) span and 36 in (0.914 m) chord, fitted with an electro-thermal ice protection system at the leading edge, for various icing conditions. The ice protection system consisted of seven heater bands, see Fig.10. Table 2 lists the wrap coordinates of each of the heaters and their individual power density. Here, *s* is the distance measured from the nose of the airfoil; a negative *s* denotes the lower surface. One particular test case is considered here, i.e. the data set referred to by Al-Khalil *et al.* as case 22A. In da Silva *et al.* [8], results obtained with the ONERA2D code are presented and compared with the experimental data from Al-Khalil *et al.* [7], the numerical results obtained with ANTICE by Al-Khalil *et al.* [7], CANICE A and CANICE B numerical results from [9] and the numerical re-

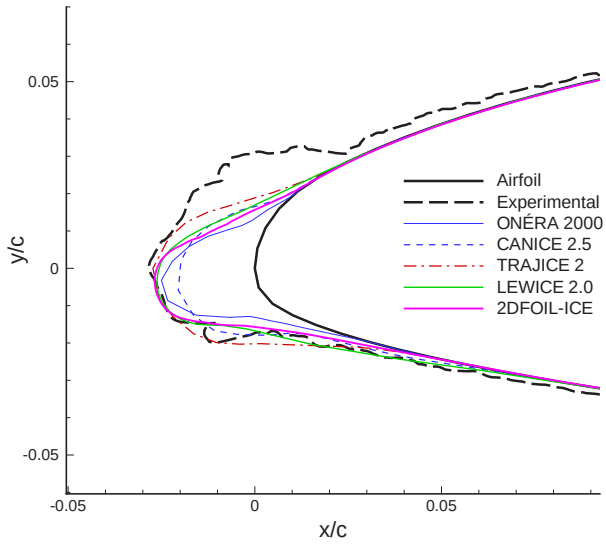

Fig. 9 The calculated ice shape for case C-9

sults from CANICE FD [10]. For the test case presented here, at 0 degrees angle of attack and with a mean volumetric droplet diameter of 20 μm, the ambient temperature is -7.6 ^{o}C, the flight velocity is 44.7 m/s and the liquid water content is 0.78 g/m^3.

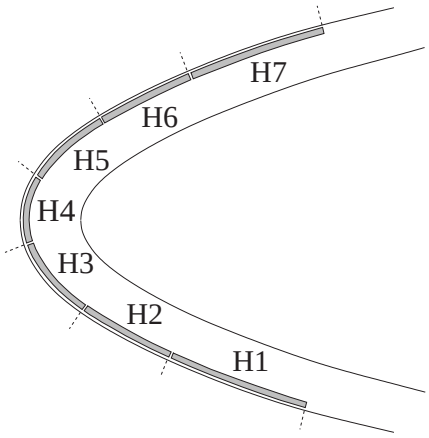

Fig. 10 Schematic of heater element placement

In the present numerical simulation, the edges of the heater elements do not necessarily coincide with the edges of the control volumes. Therefore, the code uses a linear interpolation to obtain an

Heater Element	s/c position Start	End	Power Density [kW/m^2]
H1	-0.1024	-0.0607	9.92
H2	-0.0607	-0.0329	10.23
H3	-0.0329	-0.0051	32.50
H4	-0.0051	0.0157	46.50
H5	0.0157	0.0435	18.60
H6	0.0435	0.0713	6.98
H7	0.0713	0.1129	10.24

Table 2 Power density distribution

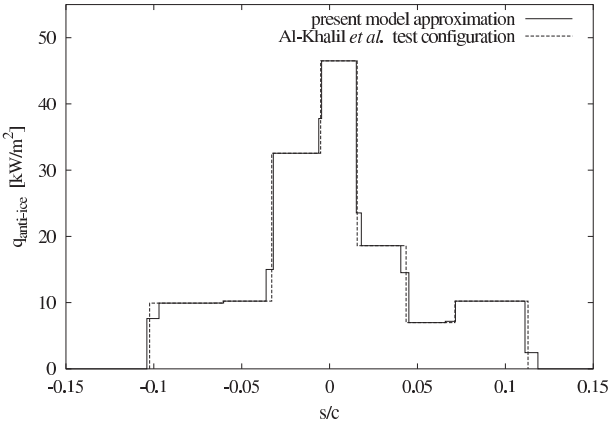

Fig. 11 Anti-ice heat flux distribution on the surface

average heat flux for each control volume, as suggested by da Silva *et al.* in [8]. The original distribution and the distribution used in the calculation are shown in Fig.11.

Furthermore, in the Frössling relations, s_{FP} has been set to $4s_C$ ($s_C/c = \pm 0.017$), so that the transition location presented by Al-Khalil *et al.* [7], $s_{turb}/c = 0.0556$, falls within the assumed transition region. $\hat{f}$ has been set to 1 in the $h_{c,BL}$ expression, Eq.(25).

The result of the flow field calculation is shown in Fig.12 in the form of a dimensionless pressure coefficient C_p,

$$C_p = \frac{p_e - p_\infty}{\frac{1}{2}\rho_a U_\infty^2} \tag{31}$$

The catching efficiency calculation follows from the droplet trajectories calculation and is shown

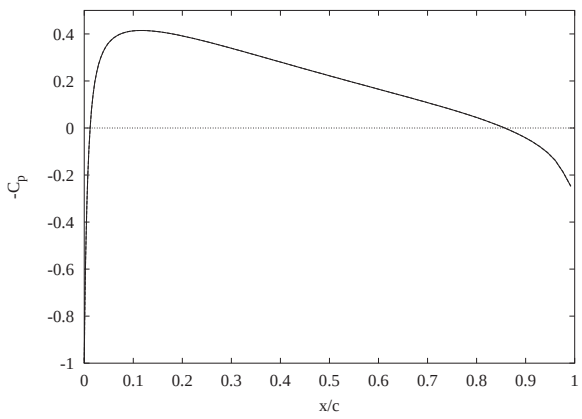

Fig. 12 Pressure distribution on NACA 0012 airfoil at α=0 º (200 panels)

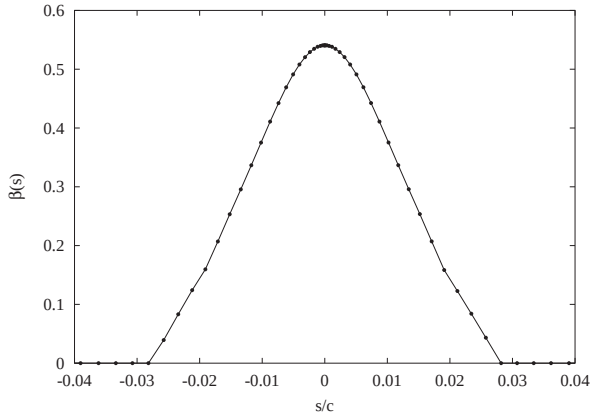

Fig. 13 β distribution. NACA 0012, α=0 º, U_∞=44.7 m/s, *MVD*=20 μm , *LWC*=0.78 g/m^3

in Fig.13, which obviously shows a symmetric distribution. The maximum value of β is 0.55 in the stagnation region. Only the first 1.6 percent of the airfoil are hit by the droplets. The convective heat transfer coefficient evaluated by the present model is shown in Fig.14. It is highest in the stagnation region, with a maximum value of around 250 W/m^{2}K. Over the rest of the airfoil the h_c is between 150 and 200 W/m^{2}K. The predicted runback water distribution is shown in Fig.15. From the stagnation point on, the amount of water increases due to the incoming droplets. A decrease sets in when the mass loss due to evaporation is higher than the mass gain by incoming droplets. The impingement limits are located at $s/c = \pm 0.028$. The runback water limits are found at $s/c = -0.031$ on the lower and $s/c = 0.033$ on the upper surface of the airfoil. Beyond these points no results are available since the analysis stops as soon as $\dot{m}_{out} = 0$. The change in slope at $s/c = 0.157$ is directly related to the location of the discontinuity in the anti-ice heat flux distribution between element H4 and H5.

The predicted solid surface temperature distribution is shown in Fig.16. It is noted that in the present study the surface temperature T_{sur} equals the solid wall temperature T_{wall}. The curve compares well with the results presented in da Silva *et al.* [8] for CANICE A, CANICE B and

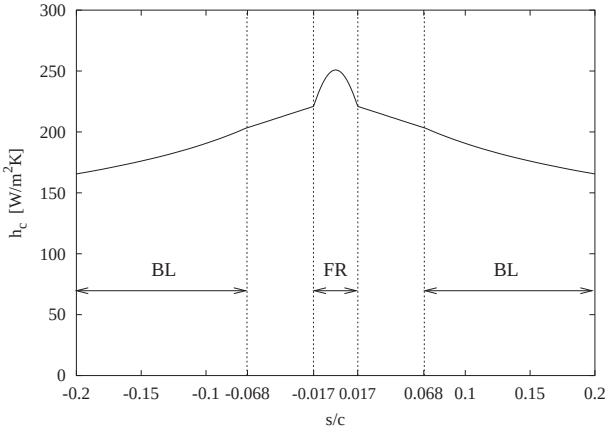

Fig. 14 Heat transfer coefficient distribution. NACA 0012, α=0 º, U_∞=44.7 m/s. FR: Frössling, Eq.(30). BL: turbulent boundary layer, Eq.(25)

ONERA2D for the region where water is still present on the airfoil. When there is no water on the metal skin, surface temperature depends strongly on the heat transfer coefficient. A better model of the heat transfer would then be needed.

Fig.16 also shows that the temperature around the stagnation point is practically constant, which justifies the use of an iso-thermal expression for the heat transfer coefficient near the stagnation point.

A calculation has been performed for the same icing conditions as used for the anti-icing case

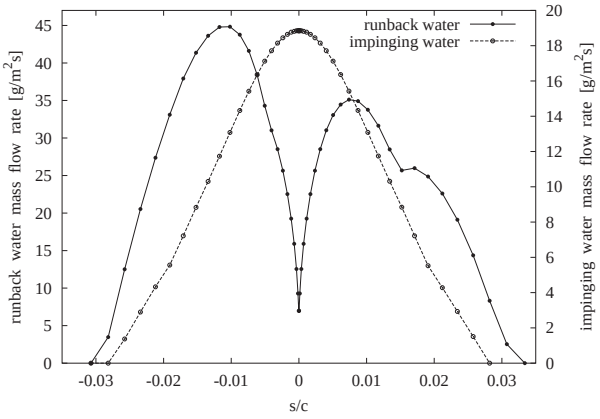

Fig. 15 Runback water mass flux $\dot{m}_{out}$ and impinging water mass flux $\dot{m}_c$. NACA 0012, α=0 °, prescribed heat flux distribution

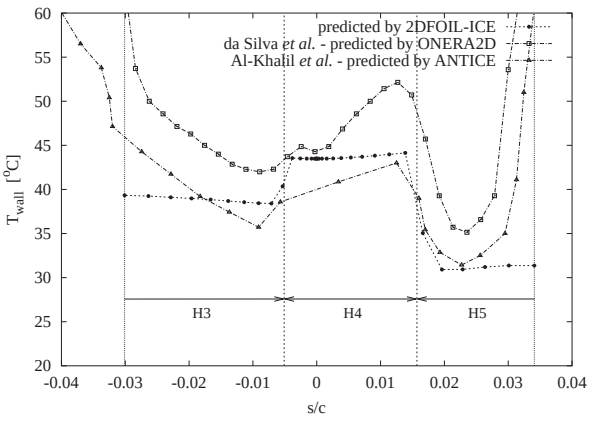

Fig. 16 Surface temperature distribution. NACA 0012, α=0 °, U_∞=44.7 m/s, T_∞=-7.6 °C, *MVD*=20 μm, *LWC*=0.78 g/m^3, prescribed heat flux distribution

presented above, but now with the surface temperature preset to a value of $T_{wall} = 1\,^{o}$C between the points $s/c = -0.018$ and $s/c = 0.018$, bounding the protected surface. Note that these boundaries are within the region of nonzero β. Fig.17 shows the calculated heat flux $\dot{Q}_{anti-ice}$, required to keep the surface temperature to the specified level of $1\,^{o}$C. The different contributions to the heat balance Eq.(24) are plotted separately in Fig.17. It shows how these terms relate to one another. The heat fluxes are given in units of [W/m^2].

It appears that water remains on the surface and flows back beyond the heated area. Fig.18 shows that runback ice has formed downstream of the protected surface.

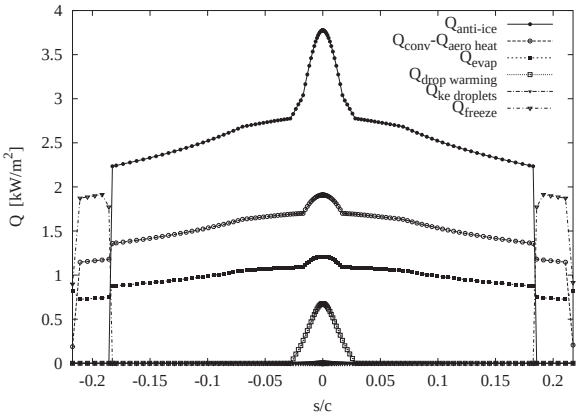

Fig. 17 Anti-ice heat flux for T_{wall}=1 °C. NACA 0012, α=0 °, U_∞=44.7 m/s, T_∞=-7.6 °C, *MVD*=20 μm, *LWC*=0.78 g/m^3

9 Conclusions

In this study, a computational method has been presented that computes ice accretion on airfoils in specified icing conditions. Calculated ice shapes have been compared with experimental results that were obtained in the NASA Glenn Icing Tunnel and with numerical results from other ice accretion prediction methods. A good agreement is found with the ice shapes predicted by other computational methods. Agreement with the experimental ice shapes is fair.

The method can be improved by implementing a better model of the external boundary layer. Solving the boundary layer equations with an integral method might give a better prediction of the friction coefficient and the heat transfer coefficient than using the local value of the velocity in the flat-plate boundary layer relations.

Also, the implementation and application of a mathematical model of a thermal anti-icing system in the ice accretion simulation method

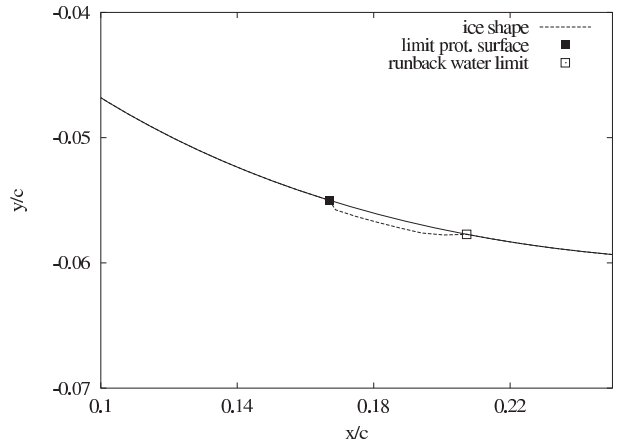

Fig. 18 Runback ice (1 min accretion). NACA 0012, α=0 °, U_∞=44.7 m/s, T_∞=-7.6 °C, *MVD*=20 μm, *LWC*=0.78 g/m^3, T_{wall}=1 °C

2DFOIL-ICE has been presented. In one case, the icing code was used to predict the surface temperature and the amount of runback water for given atmospheric conditions and heat flux distribution from an anti-icing device. In the other case, the heat requirements, to keep the surface free of ice between the limits of a user-specified protected surface, have been calculated.

Although a very basic and simplified model has been used, the computational method has proved to be able to calculate the main parameters of an airfoil anti-icing system, such as: solid surface temperatures (for the wetted region), runback water flow and convection heat transfer coefficient distributions along the external surface.

The method can be improved by applying a more sophisticated runback water model. In the present study, a velocity profile or temperature distribution in the water layer is not considered. Furthermore, a model for the internal flow and one for the heat conduction in the airfoil skin could be added.

The results obtained for both ice accretion calculation and anti-icing simulation suggest that 2DFOIL-ICE is a useful analysis tool. It also forms a test bed for carrying out more studies in order to improve the modeling of the physical processes (e.g. roughness development, heat and mass transfer, runback, splashing, droplet breakup, etc.).

10 References

[1] Snellen M, Boelens O and Hoeijmakers H. A computational method for numerically simulating ice accretion. *AIAA Paper 97-2206*, Jan. 1997.

[2] Snellen M. Ice accretion during flight. Memorandum M-749, Department of Aerospace Engineering, Delft University of Technology, Delft, The Netherlands, 1996.

[3] Messinger B. Equilibrium temperature of an unheated icing surface as a function of air speed. *J. of Aeron. Sciences*, Vol. 20, No. 1, Jan. 1953.

[4] Vukits T. Overview and risk assessment of icing for transport category aircraft and components. *AIAA Paper 2002-0811*, Jan. 2002.

[5] de Jong H. Development of a numerical method for the air flow over a thin layer of liquid. MSc Thesis, Department of Aerospace Engineering, Delft University of Technology, Delft, The Netherlands, 1995.

[6] Frössling N. Evaporation, heat transfer and velocity distribution in two-dimensional and rotationally symmetrical laminar boundary-layer flow. Technical Memorandum 1432, NACA, 1958.

[7] Al-Khalil K, Horvath C, Miller D and Wright W. Validation of NASA thermal ice protection computer codes: part III-The validation of ANTICE. *AIAA Paper 97-0051*, Jan. 1997.

[8] da Silva G, Silvares O and Zerbini E. Airfoil anti-icing system modeling and simulation. *AIAA Paper 2003-734*, Jan. 2003.

[9] Morency F, Tezok F and Paraschivoiu I. Anti-icing system simulation using CANICE. *Journal of Aircraft*, Vol. 36, No. 6, Nov.-Dec. 1999.

[10] Morency F, Tezok F and Paraschivoiu I. Heat and mass transfer in the case of an anti-icing system modelisation. *AIAA Paper 99-0623*, Jan. 1999.